# A Broadband Multi-Stage Self-Interference Canceller for Full-Duplex MIMO Radios

Haixiang Zhao, *Student Member, IEEE,* Udara De Silva, *Student Member, IEEE,* Sravan Pulipati, *Student Member, IEEE,* Satheesh B. Venkatakrishnan, *Member, IEEE,* Shubhendu Bhardwaj, *Member, IEEE,* John L. Volakis, *Fellow, IEEE,* Soumyajit Mandal, *Senior Member, IEEE,* and Arjuna Madanayake, *Member, IEEE*

***Abstract*—Full-duplex (FD) antenna arrays are desirable for expanding the channel capacity of wireless systems up to 2, which is particularly important in the crowded sub-6 GHz spectral bands. Conventional FD solutions based on circulators do not scale to antenna arrays due to the presence of significant mutual coupling between antenna elements. This paper describes a two-stage self-interference cancellation (SIC) method that is suitable for FD arrays. The first-stage SIC uses a replica antenna (RA) based network that is passive and linear, and can thus be placed before the low-noise amplifier (LNA) without significantly degrading receiver noise figure (NF) and linearity. The RA-based SIC also simplifies the hardware requirements for the second-stage SIC, which uses an analog tapped delay line (ATDL) network. The proposed two-stage SIC was realized using off-the-shelf components and tested in the 1-3 GHz range using strongly-coupled pairs of ultra-wideband antennas. Network analyzer measurements show 20-30 dB of SIC using the RA network over the entire frequency range, and $> 20$ dB of SIC using a single-stage ATDL SIC over instantaneous bandwidths of 0.53-0.65 GHz. The combined transmit-receive isolation is 66.5, 73.5, and 85.8 dB around center frequencies of 1, 2, and 3 GHz, respectively. The amount of isolation is shown to be sufficient for realizing practical FD wireless links at 2 GHz with reasonable transmit power levels (0 dBm).**

***Index Terms*—Self-interference cancellation (SIC); full-duplex antenna arrays; simultaneous transmit and receive (STAR).**

## I. Introduction

MULTI-antenna radios have multiple advantages, including directional beamforming, multi-input multi-output (MIMO) schemes, and hybrids between beamforming and MIMO. In particular, beamforming provides directed gain by maximization of the signal to interference and noise ratio (SINR) and MIMO increases capacity by diagonalization of the channel matrix. Increasing the available capacity in an array-based wireless system requires the bandwidth to be increased. However, there is extreme spectral scarcity in sub-6 GHz "legacy" bands, where bandwidth is at a premium. Although mm-wave spectrum is abundant and the future of wireless relies on moving to mm-wave bands, the legacy frequencies remain extremely important for communications due to favorable physics for highly-scattering urban environments (e.g., low path-loss). For example, the air interface standard for 5G cellular (known as 5G NR) includes multiple sub-6 GHz bands (0.6-0.7 GHz, 3.3-3.8 GHz, etc.). Full duplex (FD) radios can simultaneously transmit and receive (STAR) two different information-carrying signals over the same bandwidth, thus effectively doubling the bandwidth of operation and capacity of the wireless channel at infinite signal-to-noise

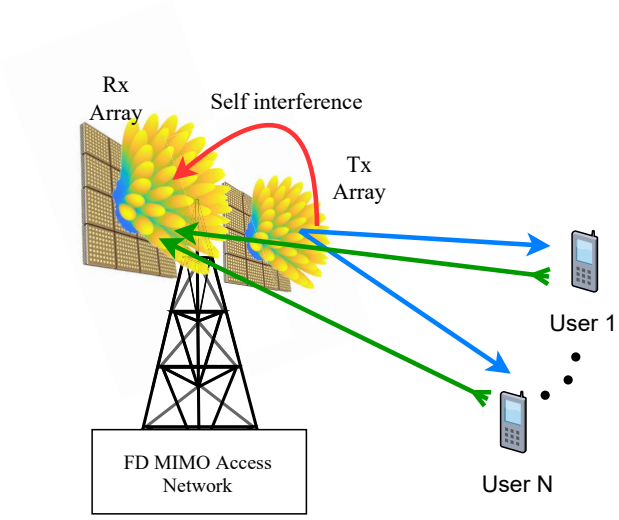


Fig. 1. Conceptual view of a full-duplex (FD) massive MIMO access point.

However, extending a single-antenna FD radio to an array-based STAR wireless system (where all the antennas in the array are in FD mode) is challenging because the transmit signal from a given antenna will radiate out and couple to all other antennas [1], as shown in Fig. 1. Each antenna is generally connected to a circulator-based duplexer to allow FD operation, which unfortunately means that the coupled signals appear in the forward paths of the receivers. These coupled signals cause self-interference as they couple into the neighboring receivers.

Thus, the fundamental problem in antenna engineering for FD arrays is mutual coupling between the array elements, which results in very high self-interference due to leakage of transmit signals into the receive paths of the coupled antenna elements. The problem is accentuated by the low-noise amplifier (LNA) and other high-gain amplifiers present at each receiver port; these amplify the mutually-coupled self-interference (SI) components by the receiver gain, which can be 90 dB or more in sensitive wireless systems. Thus, inter-element mutual coupling is the key limiting factor for

H. Zhao and S. Mandal are with the Department of Electrical and Computer Engineering, University of Florida, Gainesville, FL 32611, USA. e-mail: {haixiang.zhao, s.mandal}@ufl.edu.

Y. U. De Silva, S. Pulipati, S.B. Venkatakrishnan, S. Bhardwaj, J.L. Volakis, and A. Madanayake are with the Department of Electrical and Computer Engineering, Florida International University, Miami, FL 33174, USA. e-mail: {udesi001, spuli009, sbojjave, sbhardwa, jvolakis, amadanay}@fiu.edu.

Manuscript received October 14, 2020.

FD communications with antenna arrays [2]. Such mutually-coupled self-interference in FD arrays designed to support STAR wireless communications persists even when each element is coupled to its receiver and transmitter via an ideal 3-port circulator. The obvious solution is to use independent transmit and receive arrays that are physically separated to ensure that self-interference is sufficiently low. However, such physical separation may be infeasible in space-constrained applications.

A large amount of work exists on single-antenna wideband FD STAR systems based on various self-interference cancellation (SIC) techniques. The most common approach uses wideband circulators, for which multiple approaches to magnet-free integrated circuit (IC) realization have been explored [3]–[10]. Other approaches include polarization diversity [11]–[13] and multiple-element approaches based on orthogonal transmit/receive patterns [14], [15]. In this paper, we propose a combination of SIC methods to mitigate the problem of self-interference between transmitters and receivers in $N$-element antenna arrays. The paper builds upon our earlier work on passive broadband SIC networks [16] by i) using a multi-stage approach that provides additional cancellation, and ii) demonstrating FD operation in practical wireless scenarios.

## II. Review of SIC Techniques

Here we focus on extending FD STAR to multiple-antenna array processing, where circulators are problematic due to mutual coupling between elements. First, we review the array FD STAR problem and available solutions.

### A. Problem Definition

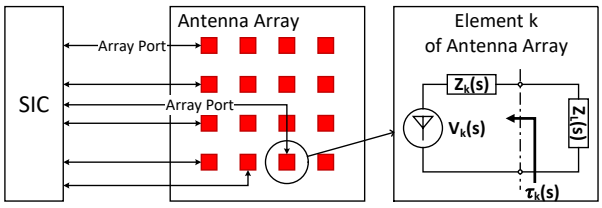


Fig. 2. Circuit model of element $k$ in an antenna array.

As shown in Fig. 2, let the array of antennas having driving point impedance functions $Z_k(s)$ be terminated by identical source impedance $Z_L(s)$ at each port of the network. The transmission coefficients at each port are

$$\tau_k(s) = \frac{2Z_k(s)}{Z_L(s) + Z_k(s)}. \tag{1}$$

Because at each port, $\tau_k$ is frequency-dependent, the incident wave $X_k(s)$ at port $k$ causes a transmitted component $X_{Tx,k}(s) = \tau_k(s)X_k(s)$. Further, at each port $k$, the antenna array produces a reflected signal $(1 - \tau_k(s))\, X_k(s)$ that travels in the opposite direction to the transmitted signals $X_{Tx,k}(s)$. Thus, the signal applied to the receivers consist of three components: 1) a desired signal $X_{In,k}(s)$, which is the incident signal from $P$ far-field sources at directions of arrival $(\theta_i, \phi_i)$, $i = 1, ..., P$; 2) an undesired signal, which is the self-interference $I_k(s)$ coupled from other antennas in the same array that are simultaneously transmitting their own waveforms $X_k(s)$; and 3) received far-signal components from other element locations due to mismatch and mutual coupling $R_k(s)$. The signals seen by receivers are therefore given as

$$X_{Rx,k}(s) = X_{In,k}(s) + I_k(s) + R_k(s), \tag{2}$$

where $I_k(s) = \sum_{u \neq k} X_{Tx,k}(s)H_{u,k}(s)$, and $H_{u,k}(s)$ are $N-1$ frequency dependent coupling functions from elements $u$ to $k$, $k = 1, 2, ..., N$, and $u = 1, 2, ..., N, u \neq k$, and $R_k(s) = \sum_{u \neq k}(1 - \tau_k(s))X_{In,u}(s)$. Here, $R_k(s)$ is the scattered and mutually coupled components of the far-field received signal from other elements that appear at element $k$.

In a typical wireless communications or radar system, the transmit signals are ~90-120 dB greater in power than received signals from the far-field. Thus, it is reasonable to assume that the self-interference (power of $X_{In,k}(s)$) is much larger than the power of mutually-coupled far-field source signals (power of $R_k(s)$). Hence the self-interference at each receiver, given by $I_k(s)$, is the primary performance bottleneck of the FD communication, as it provides very high levels of self-interference at each receiver when the transmitters connected to the antenna array are operational.

### B. Background in Network Synthesis

An $N$-element array of coupled antennas can be modeled as a passive $N$-port network [17]. For port voltage $v(t)$ and current $i(t)$, $t \in \mathbb{R}$ the instantaneous power delivered to a network $\mathbb{N}$ is defined by $p(t) \equiv v(t)i(t)$ so that the net energy delivered to the network up to time $t_0$ is $E(t_0) \equiv \int_{-\infty}^{t_0} v(t)i(t)dt$. If $E(t_0) > 0$ the network $\mathbb{N}$ has absorbed net positive energy. Passivity, activity, and losslessness are related to the ability of the network to absorb or deliver net positive energy. If $E(t_0) \geq 0$ for all possible waveforms $(v(t), i(t))$ for any $t_0$ then the network is defined as a passive network. An active network is defined as a network that is not passive. Lossless networks have $E(\infty) = 0$ where $v(t)$ and $i(t)$ are square-integrable. The concepts of activity, losslessness and passivity of a 1-port network can be extended to the multi-port case. The net energy delivered to an $N-$port network at time $t_0$ is $\Sigma_{k=1}^{N} \int_{-\infty}^{t_0} v_k(t)i_k(t)dt$. Passivity requires that for all possible $v_k(t)$ and $i_k(t)$ the net energy $E(t_0) \geq 0$, and losslessness requires that $E(\infty) = 0$ if port voltage and current waveforms are square-integrable.

A lossy passive network has a driving point impedance $Z(s)$, $s \in \mathbb{C}$ that is positive real; i.e., $\mathbb{R}[Z(s)] \geq 0$. Also, its lossy nature ensures that $E(\infty) > 0$. Circuit models of networks can be extended to 1,2, and 3-port distributed passive elements, such as microwave combiners and transmission lines. A distributed network can be modeled by selecting a suitably high-order function $Z(s)$, thus enabling the synthesis of a lumped equivalent circuit using capacitors (and/or inductors), resistors, transformers, and/or gyrators. The higher the order of $Z(s)$, the closer the fit of the synthesized equivalent circuit. For example, the $Z(s)$ of an antenna near its primary resonance can be approximated by a simple equivalent circuit (a lossy $LRC$ "tank").

Consider an $N$-port network consisting of $N$ mutually coupled antennas. From recent work [18], we know that in the receive mode such a network can be modeled with far-field sources having 377 Ω impedance (where $120\pi \approx 377$ Ω is the impedance of free space). The antenna physics, including mutual coupling of the electromagnetic fields, result in a network that is passive, with $N$ ports corresponding to the $N$ driving ports of the elements, and another $N$ "free-space ports" that can be measured [18]. Although antennas are designed for 50 Ω systems, the driving point impedance takes into account frequency-dependent positive real functions $Z_k(s), k = 1, 2, ..., N$, that capture coupling of each element to itself as well as to others. Let $Z_{A,k}(s)$ be an integer-order polynomial which is a positive real function that approximates $Z_k(s)$ to an arbitrarily small level of error (i.e., $0 \leq \|Z_k(s) - Z_{A,k}(s)\| \leq \epsilon$. Classical circuit synthesis techniques can be used to discover the interconnections and component values for the network of inductors, capacitors, resistors, gyrators and transformers required to synthesize the approximate driving point impedance functions $Z_{A,k}(s)$ to closely approximate the linear network behavior of the original distributed $N$-port passive network.

### C. Self-Interference Cancellation (SIC)

The removal of self-interference $I_k(s)$ from $X_{Rx,k}(s)$ without degrading receiver noise figure (NF) or linearity requires the subtractive cancellation of the undesired components in the analog domain using a multi-port passive RF circuit (ideally linear and noiseless) *before* the signal enters the first LNA. Let the interference-cancelled signal at antenna $k$ be denoted as $U_k(s) = X_{Rx,k}(s) - I'_k(s)$ where $I'_k(s)$ ideally would be an exact replica of the interference. When the interference can be exactly subtracted because $I'_k(s) = I_k(s)$, the residual is the sum of i) the desired far-field signal, and ii) the effects of mutual coupling on the far-field signals; for antenna $k$, it is given by $U_k(s) = X_{In,k}(s) + R_k(s)$.

Recall that at antenna $k$, the self-interference component is $I_k(s) = \sum_{u \neq k} \tau_k(s) X_{Tx,k}(s) H_{u,k}(s)$, where $H_{u,k}(s)$ are $N-1$ frequency-dependent coupling functions from elements $u$ to $k$, $k = 1, 2, ..., N$, and $u = 1, 2, ..., N, u \neq k$. The transfer functions (TFs) $H_{u,k}(s)$ depend on i) the electromagnetic coupling from each antenna to every other antenna in the array over the frequency range of interest, and ii) the driving point impedance functions of the terminations at port $k$ - which could be any microwave 1-ports (e.g., LNAs) along with impedance transformation effects due to passives, transmission line segments, or connectors. The frequency-dependent coupling between antennas makes $H_{u,k}(s)$ a high-order polynomial. The most common approach to modeling this coupling, thus allowing its removal for SIC, is an analog tapped delay line (ATDL) filter [19]. However, the high-order nature of $H_{u,k}(s)$ implies that a complex ATDL is needed to approximate it.

### D. Complexity of ATDL Self-Interference Cancellers

Let us first consider the simplest possible case where there are only two antennas in the array (i.e., $N = 2$). The coupling

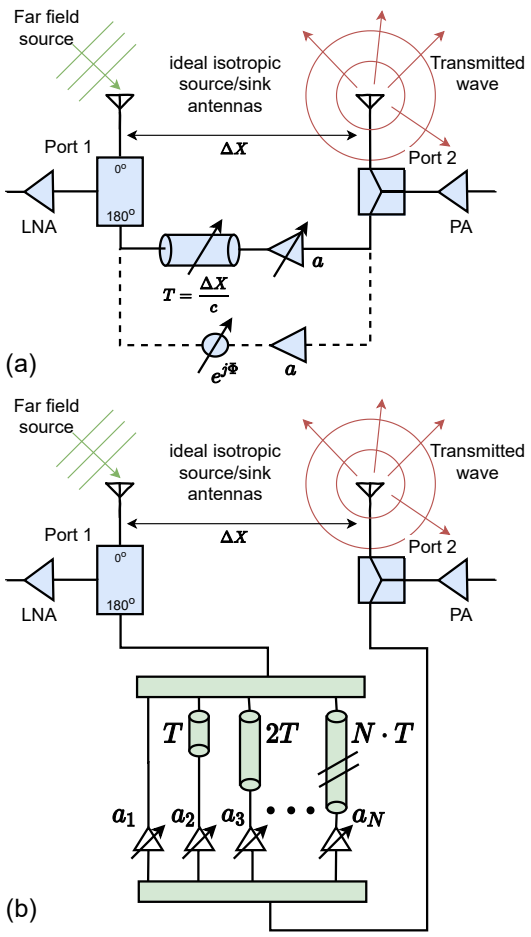


Fig. 3. (a) Single-tap and (b) multi-tap ATDL SIC.

function from antenna 2 to 1 is denoted $H_{1,2}(s)$, which is the same as the coupling from antenna 1 to 2 unless the coupling medium is non-reciprocal. Let the signal transmitted from antenna 2 be $X_{Tx,2}(s)$; the self-interference at antenna 1 due to transmission from antenna 2 is $H_{2,1}(s)X_{Tx,2}(s)$. Assuming electrically-small isotropic antennas operating at $s = j\omega$ and inter-antenna distance of $\Delta x$, the coupling function takes the form $H_{1,2}(s) = \frac{e^{-sT}}{\alpha(s)}$ where $T = \Delta x/c$, $\alpha^{-1}(\omega)$ is attenuation, and $c$ is the speed of light. Over the frequency range where $\alpha$ is approximately constant, self-interference can be removed by creating a mitigation filter having an all-pass TF $G_{1,2}(s) = H_{1,2}(s)$ and subtracting $X_{Tx,2}(s)G_{1,2}(s)$ from the signal measured at the port of antenna 1 [20]. The mitigation filter's TF can be implemented using either i) a polynomial approximation of $e^{-sT}$, or ii) a true-time delay (TTD) obtained from a segment of transmission line [20], as shown in Fig. 3. For narrowband operation, the TTD can be replaced by a phase-shifter $\phi = -\omega T$. Indeed, the narrowband case where such an assumption is valid has been solved and results are available in the literature [2]. Commercial solutions based on various narrowband ATDL SICs are also available (i.e., from Kumu Networks [21]).

A useful figure of merit for ATDL canceller designs is *delay-bandwidth product (DBP)* $T_d \times B$, where $T_d$ and $B$ are the ranges over which useful cancellation occurs as a function of coupling time-delay ($T$) and frequency ($\omega$), respectively.

For the single-tap TTD canceller shown in Fig. 3(a), only coupling due to the direct transmit-to-receive path ($Tx \rightarrow Rx$) can be cancelled, not higher-order "multi-hop" ones like $Tx \rightarrow Rx \rightarrow Tx \rightarrow Rx$; thus we get $T_d \approx T$. The resulting DBP is generally $< 1$.

Multiple versions of similar cancellers are available in the literature, notably making use of electrically balanced diplexers (EBD) for obtaining the cancellation signal [22]–[24]. The quadrature balanced power amplifier (QBPA) is a modified version of the EBD that exhibits lower Rx and Tx losses at the cost of additional hybrids and pre-amplifiers [25]. Cancellation approaches are often combined with polarization diversity to improve isolation between transmit and receive antennas [11]–[13].

### *E. Case for $N = 2$ Wideband Antenna STAR*

The extension of the above narrowband case to the wideband case using finite-sized antennas is difficult. In particular, the effects of frequency-dependent driving point impedance functions, mutual coupling effects, polarization, and frequency-dependent termination-port impedance functions (e.g., the input impedance of an LNA at antenna port 1, or the output impedance of a power amplifier (PA) at antenna port 2) makes the order of $H_{2,1}(s)$ quite high and therefore difficult to approximate using a passive network.

Higher-order ATDL-based finite impulse response (FIR) filters - also known as transversal filters - can be used for synthesizing an approximation for $H_{2,1}(s)$ for wideband operation (Fig. 3(b)). However, from the basic network theory reviewed earlier, we know that the passive multi-port networks corresponding to antenna arrays with mutual coupling contain TFs having both zeros and poles in their integer-order polynomial representations. The approximation of such coupling functions using ATDL transversal filters is possible - but the order of the corresponding FIR filter is impractically high. Consider for example a simple first-order $RC$ network. To reproduce this network's unit impulse response, an FIR filter would need to sample it at close intervals of time and use the sampled values as weights (taps) of the FIR realization. It can be shown that to achieve 1% accuracy (i.e., ∼40 dB cancellation), the FIR filter order has to be about 10. Higher-order $LCR$ networks containing about 10 inductors, capacitors, resistors, transformers and gyrators will require FIR filters of order 100-200 to obtain 1% accuracy. As a "ball park" estimate, FIR filters are about $100\times$ higher in circuit complexity compared to infinite impulse response (IIR) filters that correspond to real-world passive networks.

### *F. Challenges in Tapped-Delay Analog Filters for Large $N$*

Wideband cancellation is theoretically possible for any number of antennas. However, the required ATDL transversal filters will be of high complexity due to the high order of the resulting TFs. Further, each signal combination from antenna $u$ to $k$ where $u, k = 1, 2, ..., N$ and $u \neq k$ needs to be taken into account in the array-wide self-interference cancellation (SIC): that is, the ATDL filter circuit complexity grows at $\mathcal{O}(N^2)$. In fact, the realization of even a single high-order ATDL transversal filter for real-world antenna systems extremely challenging: in the DARPA WARP program, the approach is to use real-time learning techniques to discover about 100 filter weights for achieving SIC for a two-antenna

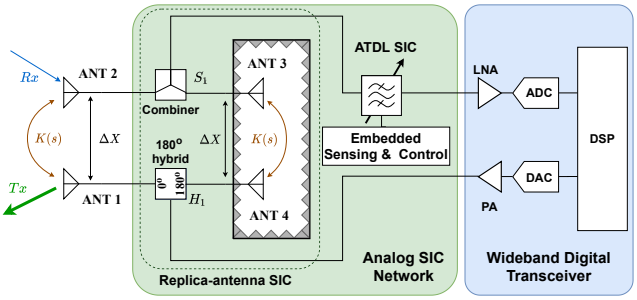


Fig. 4. Conceptual block diagram of a passive two-stage SIC network for two-antenna FD radios in which each element is in HD mode. ANT1 and ANT2 (the main array) are free to radiate, while ANT3 and ANT4 (a replica array required by the SIC) are placed inside an RF-shielded chamber.

STAR array. Even if a 2-antenna ATDL self-interference canceller can be built, scaling to a multi-antenna large-$N$ system containing hundreds/thousands of antennas, as required for 6G communications, would lead to high circuit complexity, not to mention major problems with noise, distortion, limited dynamic range, and high power consumption.

Although techniques borrowed from digital FIR filter theory, such as common sub-expression sharing, can be used for significantly reducing circuit complexity of ATDL SIC approaches, when the number of antennas is large, the circuit complexity is still significant [26]. Thus, wideband self-interference cancellation for a large number of elements using ATDL filter circuit-based interference subtraction is prohibitively difficult in realize from a practical standpoint.

In our proposed approach, the near-field mutual coupling is first subtracted passively across all antennas in the array, over extremely wide bands, using a noise-less, distortion-free passive network. Low-order ATDL filters are used only for second-level SIC and cancelling multipath reflections from the environment. Therefore, our approach leads to low active circuit complexity.

## III. Passive Replica-Antenna SIC

We begin by considering two-antenna FD transceivers in which each element is in half-duplex (HD) mode (i.e., either transmitting or receiving) and the two antennas are separated by a (small) distance $\Delta x$. This configuration can be viewed as an important first step towards realizing true FD antenna arrays where each element is in FD mode. We developed a two-stage SIC for such systems: i) a broadband canceller based on a passive microwave network; and ii) a low-order adaptive ATDL filter using tapped delay lines. The former uses a 6-port network and a physically-identical replica antenna array ($N = 2$) inside an RF-shielded chamber, as shown in Fig. 4.

The proposed passive SIC concept can be analyzed by considering signal flows within the transceiver system shown in Fig. 4. The most challenging aspect is to create an exact copy of the interfering signal. Here, such a copy is generated

through the replica antennas ($ANT_3$ and $ANT_4$), which ideally have the same inter-antenna coupling as the main antennas ($ANT_3$ and $ANT_4$). However, they are placed in a miniature radio-silent environment (shielded box) to prevent them from receiving external signals.

Assuming good matching between the main and replica antenna arrays, the mutual coupling between each pair of antennas is described by the frequency-dependent input-output TF $T' = K(s)$. The 180° hybrid $H_1$ splits the transmit signal into two out-of-phase parts, one of which is fed into the main transmit antenna ($ANT_1$) and the other to the replica transmit antenna ($ANT_4$). As a result, the transmit signal $x$ appears inside the RF shielded box as $-x$. Thus, the self-interference component in the receive path becomes $T'x$ for the main array (facing the far-field) and $-T'x$ for the replica array (within the RF-shielded box). The frequency-independent nature of the signal inversion (which arises from the matched mutual coupling functions of the main and replica arrays) ensures broadband cancellation when the two self-interference terms are added up by the combiner $S_1$ in the receive path. Thus, mutual coupling-induced self-interference is strongly suppressed in the input signal to the receiver LNA. Such a passive (and ideally noiseless) network, which we refer to as a *replica-antenna SIC*, can be used in front of a tunable ATDL canceller to provide a significant amount of initial SIC that drastically simplifies the required ATDL network.

### A. Performance Analysis

The main performance limitations of the proposed replica-antenna SIC include: i) a 3 dB loss of transmit power, since half the input power is fed into the dummy antennas; ii) a 3 dB increase in receiver noise figure (NF) due to the insertion loss (IL) of the 180° hybrid; and iii) the cost and component count/weight associated with the replica antennas and RF-shielded box. In addition, the amount of SIC is limited by the amplitude and phase imbalances of the 180° hybrid and combiner. The frequency dependence of these imbalance terms ultimately limits the useful cancellation bandwidth of the network.

Theoretically, our proposed SIC has at least 3 dB loss in both Tx and Rx paths. It is useful to compare this with similar work that uses circulators, EBDs, or QBPAs as primary isolation devices, along with ATDLs or other structures for providing secondary isolation. The proposed RA has the same Rx/Tx-loss as an EBD due to the fact that they both use 3 dB hybrids and splitters to combine/split the SI and SIC signals. In addition, unlike circulator or QBPA-based SICs, the Tx/Rx-loss of both EBDs and RAs is independent of the antenna reflection coefficient [27]. Thus, the proposed RA SIC most closely resembles an EBD. The key difference is that the necessary balancing impedance is automatically provided by the replica antenna array (instead of being emulated by a complex lumped network), which allows our method to easily scale to larger arrays.

The channel capacity of the original transceiver is defined by $C = B \cdot \log_2\left(1 + 10^{SNR_0/10}\right)$, where $B$ is the channel bandwidth and $SNR_0$ is the received SNR. After using our proposed SIC system, the bandwidth $B$ expands to $2B$ due to FD operation, while $SNR_0$ decreases by ∼6 dB for a given PA output power level (due to 3 dB losses in both Tx and Rx). Thus, the new channel capacity becomes $C' = 2B \cdot \log_2\left(1 + 10^{(SNR_0-6)/10}\right)$. Fig. 5 plots the ratio $C'/C$ versus $SNR_0$. This figure shows that $SNR_0 > 8$ (i.e., 8.95 dB) is required for $C'/C$ to exceed 1, i.e., for the proposed SIC to provide increased channel capacity. However, note that channel capacity is not the only potential advantage of FD operation. For example, communication latency, which is one of the critical requirements for next-generation wireless standards (e.g., 5G/6G cellular) can be significantly reduced by switching from HD to FD.

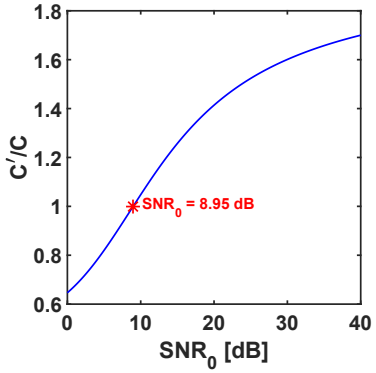


Fig. 5. Channel capacity ratio between a FD communication system using our proposed SIC, and a conventional HD system operating over the same bandwidth.

### B. Design of the RF-Shielded Chamber

An RF-shielded chamber is critical to ensure that the replica antenna array only sees the self-interference signal. Such chambers use walls that are lined with an RF absorber. To minimize the effects of this lossy layer on antenna characteristics, the walls are typically placed in the far-field, i.e., at a distance of several times the maximum RF wavelength of interest (denoted by $\lambda_{max}$). The resulting box volume scales as $\lambda_{max}^3$, and thus may become prohibitively large at lower frequencies. Thus, reducing the size of the chamber is of importance from a practical standpoint. This may be accomplished by using dielectric loading to reduce $\lambda_{max}^3$ for a particular frequency range. Inside the RF-shielded box, both magnitude and phase components of the mutual coupling TF $T'$ are identical to values in air if i) the antennas are placed in a dielectric medium with relative permittivity $\epsilon_r$, and ii) antenna geometry and array spacing are reduced by $\sqrt{\epsilon_r}$. Using such a *dielectric-scaled chamber* results in a volume reduction of $(\epsilon_r)^{3/2}$, as shown in Fig. 6. For example, $\epsilon_r = 4$ would imply a $8\times$ volume reduction of the RF-shielded box compared to an air-filled version.

### C. Extension to FD Arrays

The proposed replica-antenna SIC can be modified to enable FD antenna arrays, i.e., arrays in which each element operates

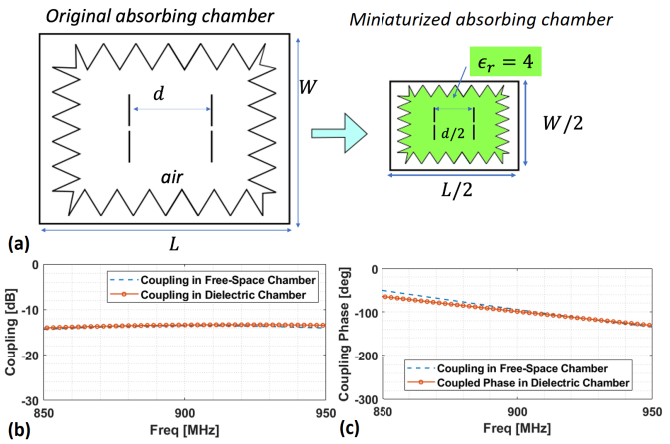


Fig. 6. (a) An RF-shielded chamber filled with a medium of dielectric constant $\epsilon_r$ (solid, liquid or gas) allows a volume reduction of $(\epsilon_r)^{3/2}$. (b)-(c) Comparison of the simulated mutual coupling TF between two antennas in the original (air-filled) and miniaturized (dielectric-scaled) chambers.

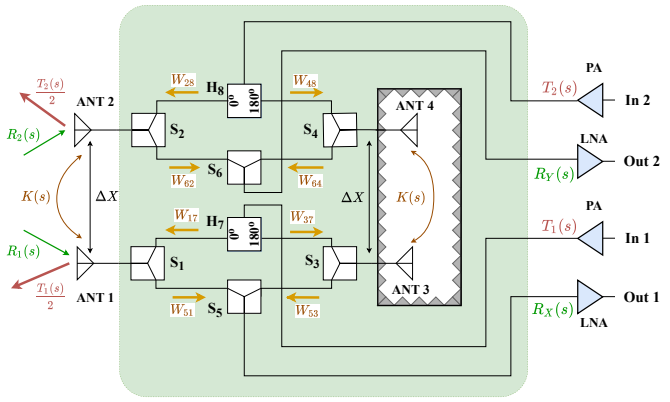


Fig. 7. Modified replica-antenna SIC for two-element FD arrays that support full $2 \times 2$ MIMO.

in FD mode. An $N$-element array of this type would enable FD $N \times N$ multiple-input multiple-output (MIMO) wireless systems. We explain the concept using the $N = 2$ case, for which the modified SIC is shown in Fig. 7.

Let the transmit signal at Input 1 be $T_1(s)$. The 180° hybrid $H_7$ splits this signal into $W_{17}$ and $W_{37}$ components such that $W_{17} = -W_{37} = T_1(s)/\sqrt{2}$. At the combiner $S_1$, $1/\sqrt{2}$ of the power in $W_{17}$ is sent to $ANT_1$ and some power leaks into $W_{51}$, as follows:

$$W_{51}(s) = \frac{R_1(s)}{\sqrt{2}} + W_{17}(s)P(s) + \frac{T_2(s)}{2}K(s) + \frac{T_1(s)}{2}J(s), \tag{3}$$

where $R_1(s)$ is the desired signal received by $ANT_1$, $P(s)$ represents the combiner leakage, $K(s)$ represents the mutual coupling between $ANT_1$ and $ANT_2$, and $J(s)$ represents the antenna return loss. Due to the symmetry of the design, the effects of $P(s)$, $K(s)$, and $J(s)$ are present in $W_{53}(s)$ as well:

$$W_{53}(s) = W_{37}(s)P(s) - \frac{T_2(s)}{2}K(s) - \frac{T_1(s)}{2}J(s). \tag{4}$$

At the $S_5$ splitter, $W_{51}(s)$ and $W_{53}(s)$ are combined to produce Output 1, denoted by $R_X(s)$:

$$\begin{aligned} R_X(s) &= W_{51}(s) + W_{53}(s) \\ &= \frac{R_1(s)}{2} + (W_{17}(s) + W_{37}(s))\,P(s). \end{aligned} \tag{5}$$

Ideally, $W_{17}(s) = -W_{37}(s) = T_1(s)/\sqrt{2}$, so self-interference is cancelled and $R_X(s) = \frac{R_1(s)}{2}$. Similarly, it can be shown that Output 2 is $R_Y(s) = \frac{R_2(s)}{2}$. Thus, the modified network has a minimum insertion loss (assuming no additional losses in the coupler and hybrid) of 6 dB for both Tx and Rx paths, which is 3 dB larger than for the simpler network in Fig. 4.

The insertion loss of the modified SIC can be significantly improved by replacing power splitters $S_1$-$S_4$ with circulators. However, commercial circulators are narrowband. Hence they will limit the overall bandwidth of the system. Emerging wideband active circulators [3], [28], [29] are promising alternatives to power splitters, since they can provide both low insertion loss and wideband operation.

The proposed SIC approach can be extended to any number of antennas in a straightforward manner. The design requires three combiners and one 180° hybrid for each antenna, resulting in a linear increase of system complexity with array size. Note that this is only possible because the replica array efficiently replicates the entire $N \times N$ mutual coupling matrix of the array (including both short- and long-range coupling). Therefore, the proposed SIC network is suitable for flexible and low-cost FD MIMO systems.

## IV. Programmable ATDL SIC

The proposed replica-antenna SIC structures (shown in Figs. 4 and 7) are linear, ultra-broadband, and noiseless, which makes them ideal for initial (first-level) SIC. However, their effectiveness is limited by i) matching between the main and replica antenna arrays, and ii) amplitude and phase mismatches in the combiners and hybrids. Thus, they need to be combined with additional SIC stages based on ATDL networks and/or digital filters to obtain enough cancellation (90 dB or more) for practical FD operation.

### A. ATDL Design

We add directional couplers to the replica-antenna canceller to enable second-level SIC using an ATDL network, as shown in Fig. 8 for a basic two-antenna FD radio (with each element in HD mode). The couplers $C_3$ and $C_4$ sample the unwanted self-interference transmit signal for use by later SIC stages, while $C_1$ and $C_2$ are dummy devices that maintain the symmetry of the connections to the main and replica arrays.

We used the sampled signals available from the couplers to implement a two-tap ATDL canceller, as shown in Fig. 8. The first tap uses i) a broadband LNA to amplify the receiver output (containing self-interference), and ii) a programmable attenuator ($ATT_1$) and delay line ($D_1$) to scale and time-delay a copy of the transmit signal (obtained using the directional coupler $C_4$). The two signals are subtracted from each other using a 180° hybrid ($H_2$) to realize SIC. The second tap uses the same cancellation approach, but derives its copy of the transmit signal from the directional coupler $C_3$.

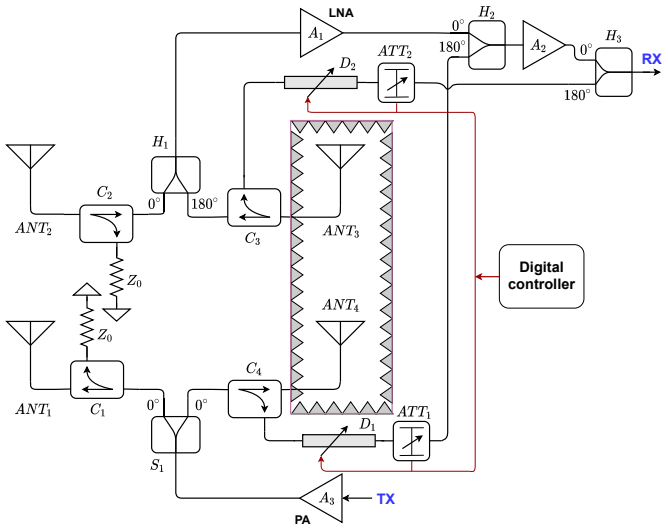


Fig. 8. Schematic of a practical two-stage SIC system for a two-element FD radio ($N = 2$) in which each element is in HD mode. The two key components are i) first-stage SIC based on a replica-antenna network, and ii) second-stage SIC based on a programmable ATDL network. $C_i$ = directional couplers, $H_i = 180°$ hybrids, $S_i = 0°$ splitter, $D_i$ = programmable time delay, $ATT_i$ = programmable attenuator.

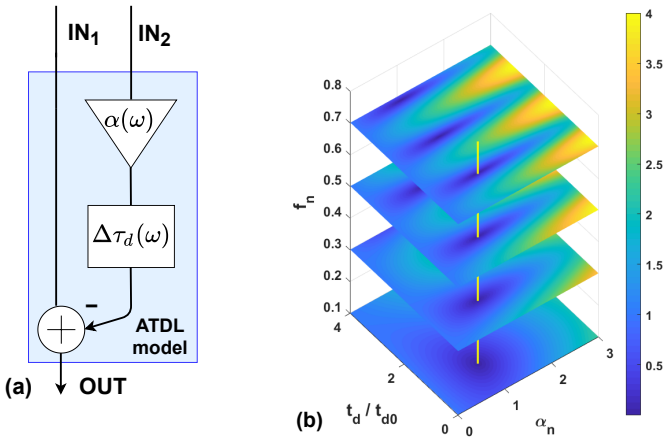


Fig. 9. (a) Block diagram of a single-stage ATDL canceller, and (b) its theoretical 3-D transfer function as a function of time-delay mismatch, amplitude mismatch, and frequency. The vertical line represents the ideal case (no mismatch), for which broadband cancellation is obtained.

### B. Performance Analysis

The ideal signal and interference TFs of each two-input, one-output ATDL tap are frequency-independent and equal to $H_S = 1$ and $H_N = 0$, respectively. However, in practice there are frequency-dependent mismatches between the amplitudes and time delays of the two signal paths within each tap (e.g., due to the finite bandwidth of the LNA). These mismatches, which are denoted by $\alpha_n(\omega) \neq 1$ and $\Delta t_d(\omega) \neq 0$, respectively, result in an interference TF of

$$H_N(\omega) = 1 - \alpha_n(\omega) e^{-j\omega\Delta t_d(\omega)}, \tag{6}$$

as shown in the signal-flow graph of Fig. 9(a). This function only approaches zero over a limited frequency range, as shown in Fig. 9(b). Thus, one of the key issues with ATDL cancellers is limited instantaneous bandwidth (IBW) for self-interference cancellation. Fortunately, the use of digitally-programmable attenuators and delay lines allows the SIC frequency response to be adaptively tuned over a much broader range, as indicated in Fig. 8.

## V. Experimental Results

### A. Antenna Array Design

Tests were conducted using identical planar ultra-wideband (UWB) antennas on a printed circuit board (PCB). The elements are circular in shape (diameter = 4 cm) and have a relatively small center-center separation of $\Delta x = 5.3$ cm ($0.18\lambda$ - $0.53\lambda$ in the 1-3 GHz range), resulting in significant mutual coupling. Two nominally identical boards were used to realize the main and replica arrays, respectively. We also built a miniature shielded chamber (outer dimensions $= 25 \times 35 \times 20$ cm) using RF absorber panels (MF22-0009-00, MAST Technologies) to surround the replica array, as shown in Fig. 10(c). The absorber panels are of the lossy foam type and have an insertion loss of 20 dB/cm.

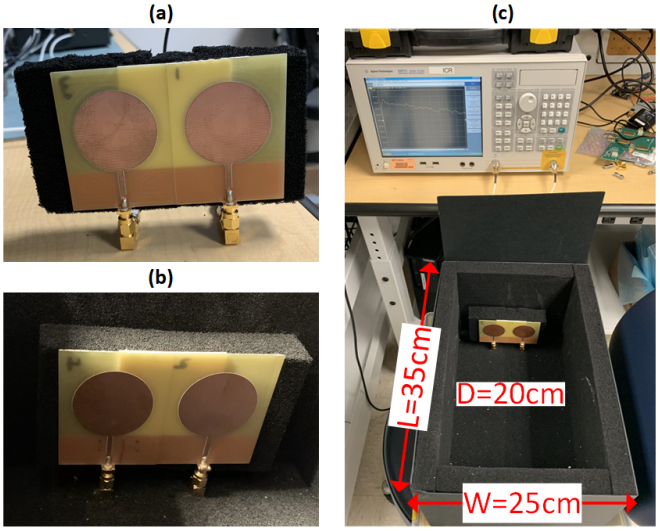


Fig. 10. Photos of antenna arrays: (a) main antennas; (b) replica antennas. (c) EM-shielded chamber used for isolating the replica antennas from the external wireless environment, with the lid open to show internal details.

Fig. 11 summarizes the measured reflection and transmission coefficients of all four antennas from 0.8-3.1 GHz. The coefficients (and thus, the terminal impedances and mutual coupling) of the main antennas ($ANT_{1,2}$) are in good agreement with those of the replica antennas ($ANT_{3,4}$), particularly above 1.5 GHz. This result confirms that the network properties (i.e., the $S$-parameter matrix) of the main antennas are being accurately reproduced by the replica antennas, as desired. It also suggests that a shielded enclosure with dimensions $\approx \lambda_{max}$ is sufficiently large for this application; note that this is significantly smaller than typical anechoic chambers.

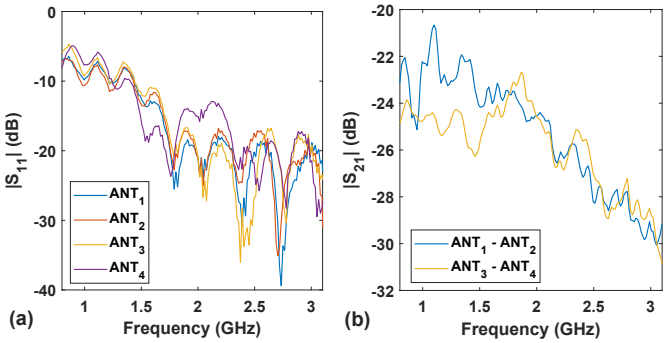


Fig. 11. Measured (a) reflection coefficients, and (b) mutual coupling for the main antennas ($ANT_{1,2}$) and replica antennas ($ANT_{3,4}$).

### B. Replica-Antenna SIC

We realized an experimental prototype of the two-stage SIC design shown in Fig. 8. Our prototype integrates all the required components of the first-stage replica-antenna SIC on the board level (Fig. 12(a)), while connectorized components are used for the second-stage ATDL SIC (Fig. 12(b)). The main components, all of which were selected to provide at least 1-3 GHz bandwidth, included: i) Mini-Circuits SYPS-2-33+ and ZX10-2-252-s+ (0° splitters/combiners); ii) Mini-Circuits SYPJ-2-33+ (180° hybrid); iii) Mini-Circuits BDCH-25-33+ (directional coupler with 25 dB coupling factor); iv) Mini-Circuits ZX60-83LN-S+ (broadband LNA); v) Mini-Circuits ZX76-31R75PP-S+ (programmable attenuator with 7-bit digital control); and vi) GigaBaudics QPADL6 (programmable 4-channel delay line with 7-bit digital control). This section focuses on validation of the replica-antenna SIC using this setup, while the next section focuses on the ATDL SIC.

Since the replica-antenna SIC has no active components, its performance can be evaluated by directly comparing the mutual coupling (i.e., the value of $|S_{21}|$ from a network analyzer measurement) with and without the replica antennas. The measured performance of the experimental prototype is shown in the frequency domain (1-3 GHz) in Fig. 13(a). The direct antenna coupling (without any cancellation) ranged from $-18$ to $-25$ dB in the 1-3 GHz band; the proposed analog SIC canceller improved this by $> 20$ dB over the entire range (residual SIC of $-45$ to $-60$ dB). The "improvement" shown in the figure is defined as the difference between $|S_{21}|$ with and without the canceller. By this definition, a negative value means that the canceler provides less mutual coupling when inserted into the system. Also, $|S_{21}|$ while using the canceller can be found by summing the improvement curve and the original $|S_{21}|$.

We also consider the channel impulse responses (from transmitter to receiver) with and without the replica-antenna SIC. These functions were estimated by computing the inverse Fourier transform of the frequency-domain mutual coupling data, and the results are shown in Fig. 13(b). The short-term response (0-20 ns), which is dominated by direct inter-antenna coupling, is significantly reduced by the canceller, as expected. As a result, the replica-antenna canceller has high DBP. In fact, since our measurements show 20 dB SIC from 0-15 ns over a 2 GHz bandwidth, DBP $\approx$ 30. This result highlights the potential of the proposed passive SIC approach in FD STAR arrays for future wireless and radar systems.

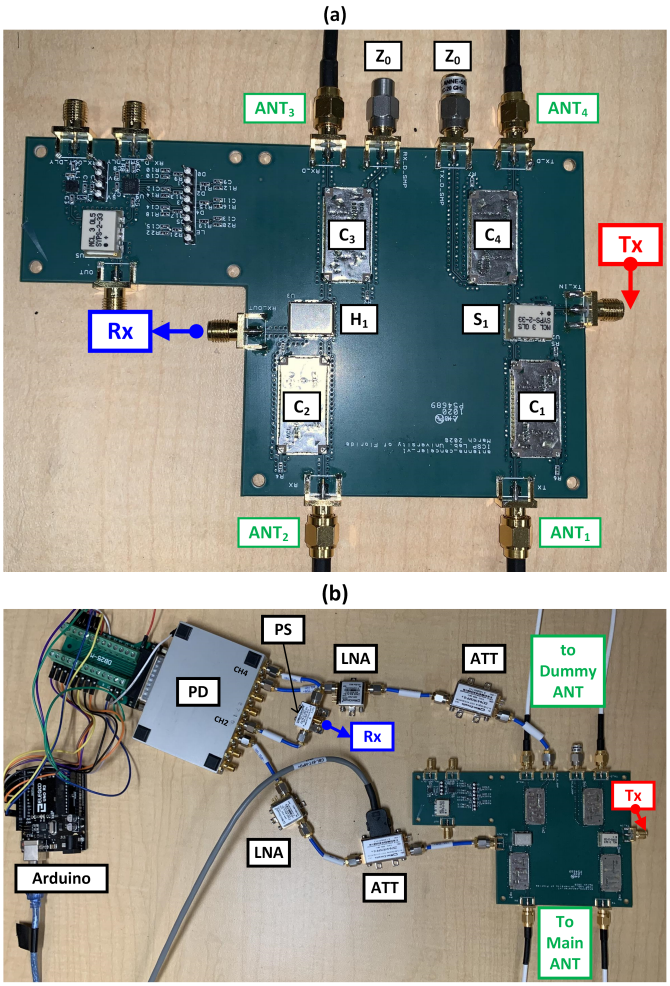


Fig. 12. (a) Photograph of the first stage of SIC system, labeled according to Fig. 8. (b) Photograph of the entire two-stage SIC system. ATT = programmable attenuator; PS: power splitter/combiner; PD: programmable time delay.

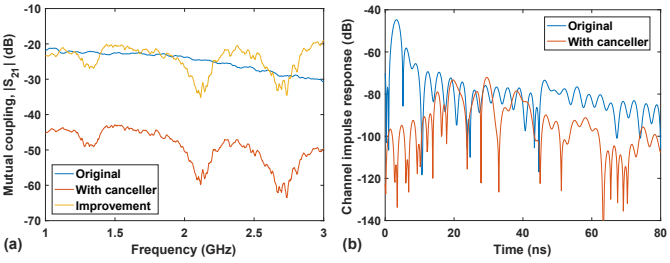


Fig. 13. (a) Measured SIC performance of the replica-antenna SIC. A transmit-receive isolation of 45-60 dB (20-30 dB improvement) is achieved from 1-3 GHz. (b) Time-domain channel impulse response estimated from the frequency-domain data in (a), showing significant reduction in short-range coupling (0-20 ns).

### C. ATDL SIC

In this section, we describe how the replica antenna SIC can be combined with an ATDL for additional SIC. The need

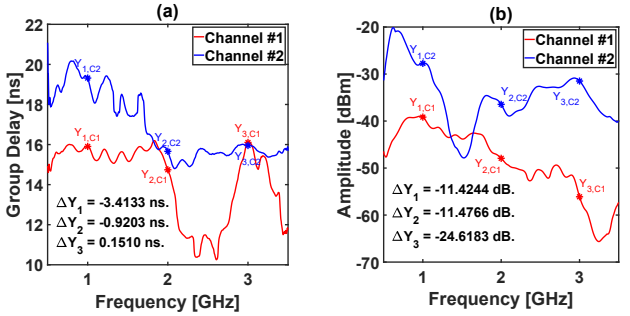


Fig. 14. Measured transmission coefficients ($S_{21}$) from the transmit port to the two ATDL signal paths before programming the ATT and PD (both were kept at their initial digital state of 0x00): (a) group delay and (b) log-magnitude. The values of group delay and coupling magnitude obtained at three selected frequencies (1, 2, and 3 GHz) are also labeled on the plots.

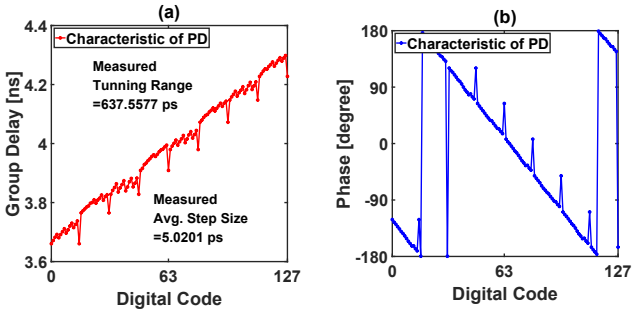


Fig. 15. Measured group delay and phase shift (at 2 GHz) between input and output ports as a function of the digital code for one channel of the PD used to implement the ATDL SIC.

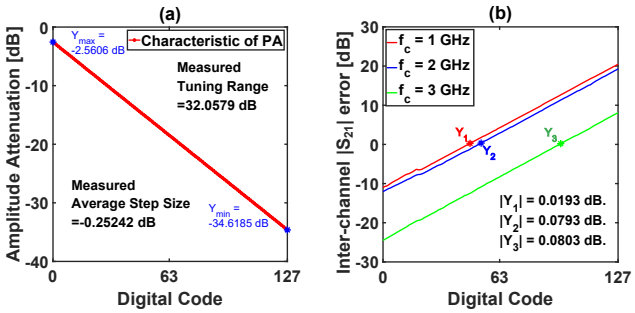


Fig. 16. (a) Measured insertion loss ($|S_{21}|$ at 2 GHz) of the programmable attenuator (ATT) as a function of its digital code (from 0x00 to 0x7F). (b) Measured difference in insertion losses ($|\Delta S_{21}|$) between the two paths in the ATDL tap at various frequencies as a function of the ATT control code. The PD control code was kept fixed at its initial state (0x00).

for a programmable attenuator (ATT) and time delay (PD) to obtain good SIC from the ATDL is highlighted in Fig. 14. This figure shows the measured transmission coefficients from the transmit port to the two signal paths within one ATDL tap as a function of frequency. Both the group delays and magnitudes of these paths have to match to cancel the self-interference term. However, we observe frequency-dependent mismatches between both delays ($\Delta\tau_d(\omega)$) and magnitudes ($\alpha(\omega)$). These mismatches can be removed around a particular frequency by programming the ATT and PD components, resulting in SIC over a certain bandwidth. Note that the cancellation bandwidth is limited by the rate at which these mismatches vary with frequency, i.e., $\partial(\Delta\tau_d)/\partial\omega$ and/or $\partial\alpha/\partial\omega$. Thus, cancellation bandwidth can be maximized by using ultra-broadband components (ideally, with frequency-independent group delay and gain) within the SIC.

The measured group delay and phase shift (at 2 GHz) of the PD as a function of its digital control input are shown in Fig. 15. The PD uses GaAs switches to connect small on-board transmission line segments in series, resulting in a broadband response (DC-6 GHz), low noise, and high linearity ($P_{1dB} > 24$ dBm). The average delay step size is $\Delta\tau = 5.0$ ps (corresponding to a relatively small phase step of $\Delta\phi = 5.4°$ at the maximum target frequency of 3 GHz), while the total delay tuning range is 0.64 ns. However, the delay tuning curve is non-monotonic and suffers from significant differential nonlinearity (DNL) at major digital code transitions (e.g., from 63 to 64); the delay programming algorithm is designed to avoid these transitions.

Fig. 16(a) shows the measured insertion loss (at 2 GHz) of the programmable attenuator (ATT) as a function of its digital control unit. A linear-in-dB response with a control range of ∼32 dB and a step size of 0.25 dB is observed. This range is sufficient to obtain SIC over a broad frequency range, as shown on Fig. 16(b). This figure shows the difference in insertion losses between the two signal paths in the ATDL as a function of the ATT code at three frequencies: 1, 2, and 3 GHz. In each case, the difference can be minimized to $< 0.08$ dB by optimizing the ATT code.

After applying the optimal ATT code values, the remaining error between the two signal paths arises from time delay error $\Delta\tau_d$, which was estimated using more network analyzer measurements. The optimal PD code values for removing this error were then predicted from PD characterization data (for example, that shown in Fig. 15). The optimal sets of digital codes for 1, 2, and 3 GHz were then stored in a lookup table; additional frequencies can be added to this table if needed.

The measured coupling between transmit and receive ports at 1, 2, and 3 GHz was measured after applying the optimal code values predicted by the lookup table. Note that these measurements include the gain of the receive path in the ATDL, consisting of LNA gain (approximately 21.8-22.1 dB) and loss of the 180° hybrid (approximately 3.6-4.4 dB). Thus, the transmit-receive (Tx/Rx) isolation is approximately 17-18 dB smaller than the measured mutual coupling ($|S_{21}|$); the results are shown in Fig. 17. The measurements show that, in each case, the ATDL provides ∼20 dB of additional SIC over a relatively broad frequency range (−3 dB bandwidths of 530-860 MHz). Additional measurements (not shown) show that matching only the phases (and not the group delays) of the two signal paths provides similar levels of SIC, but over less than half the bandwidth; increased cancellation bandwidth is a well-known advantage of TTD cancellers [20].

Table I summarizes the measured performance of the two-stage SIC. After correcting for receiver gain, the Tx/Rx isolation (at the target frequency) increases from −66.5 dB to −85.8 dB as we go from 1-3 GHz; this trend is mostly explained by i) better matching between the main and replica

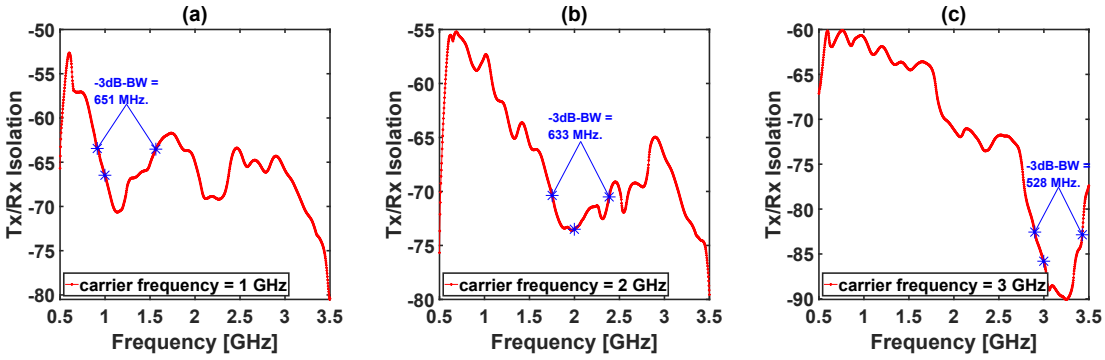


Fig. 17. Measured transmit-receive isolation versus frequency for the two-stage SIC (including the gain of the receive path) with the ATT and PD tuned for maximum cancellation at (a) 1 GHz, (b) 2 GHz, and (c) 3 GHz. In each case, the target frequency and $-3$ dB cancellation bandwidth are marked on the plots.

antenna pairs (Fig. 11), and ii) better isolation between the antennas in each pair (Fig. 13). Also note that only a single-tap ATDL was implemented during these measurements; adding the second ATDL tap available in the system (as shown in Fig. 8) is expected to provide 15-20 dB of additional SIC.

TABLE I
MEASURED PERFORMANCE OF THE TWO-STAGE SIC

| Center freq. $f_c$ (GHz) | Mutual coupling (at $f_c$) | Tx/Rx isolation (at $f_c$) | $-3$ dB BW (GHz) |
|---|---|---|---|
| 1 | $-48.3$ dB | $-66.5$ dB | 0.65 |
| 2 | $-55.4$ dB | $-73.5$ dB | 0.63 |
| 3 | $-68.7$ dB | $-85.8$ dB | 0.53 |

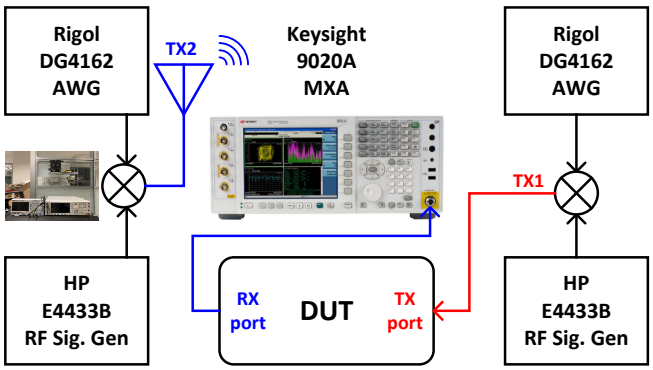


Fig. 18. Test setup used for FD wireless experiments. DUT = device under test (the local transceiver); AWG = arbitrary waveform generator; MXA: RF signal analyzer.

### D. FD Wireless Experiments

We carried out a set of FD experiments using the wireless test setup shown in Fig. 18 to demonstrate the benefits of the proposed low-complexity two-stage SIC network. Two modulated RF sources (denoted by TX1 and TX2) were created by driving the I-Q modulation ports of two RF signal generators (Agilent/HP E4433B) with dual-channel arbitrary waveform generators (Rigol DG4162). The first ("local") source was connected to the transmit port of the dual-antenna system, while the second ("remote") source was connected to a single ultra-wideband antenna placed at a distance of 1.5-3 m. Finally, the receive port of the dual-antenna system was connected to an RF signal analyzer (Agilent/Keysight 9020A) with digital demodulation capabilities, thus completing the local transceiver.

Next, we present typical experimental results obtained from the wireless test setup from 1-3 GHz. In initial tests, the remote transmitter (TX2) was set up to generate an AM-modulated waveform, while the local transmitter (TX1) was set up in continuous wave (CW) mode. Received spectra in three cases (no SIC, only the replica antenna [RA] SIC, and the two-stage SIC) are shown in Fig.19. In each case, the frequency of TX1 (i.e., the self-interference) was chosen such that its spectrum overlapped one of the modulated sidebands of TX2 (i.e., the received wireless signal). The figure shows 17-22 dB and $\sim$18 dB of SIC from the RA and ATDL networks, respectively; these results are in good agreement with the network analyzer measurements.

In the next experiment, we consider a more practical scenario in which TX1 and TX2 are digitally modulated using QPSK and QAM16, respectively, at a symbol rate of 1 MS/s. Fig. 20 show the measured spectra from the receive port in three cases (no SIC, only the RA SIC, and the two-stage SIC) when the two transmitters have a moderate frequency offset (3 MHz in this experiment). As expected, the self-interference (TX1) dominates the received signal when no SIC is used. The two-stage SIC provides $> 40$ dB of cancellation, such that the received signal is dominated by the remote transmitter (TX2).

The next experiment considers the more challenging scenario in which TX1 and TX2 are still digitally modulated using QPSK and QAM16, respectively, but now have the same carrier frequency, resulting in true FD operation. The results are shown in Fig. 21 for a fixed TX1 symbol rate (1 MS/s) and different TX2 symbol rates (0.5, 1, and 2 MS/s). In each case, the spectra show that self-interference from TX1 is effectively removed when the RA and ATDL networks are combined, thus enabling FD operation.

In the final experiment, we characterized the received signal constellations in FD mode without and with the proposed SIC. The results are shown in Figs. 22, 23, and 24. Figs. 22(a)-

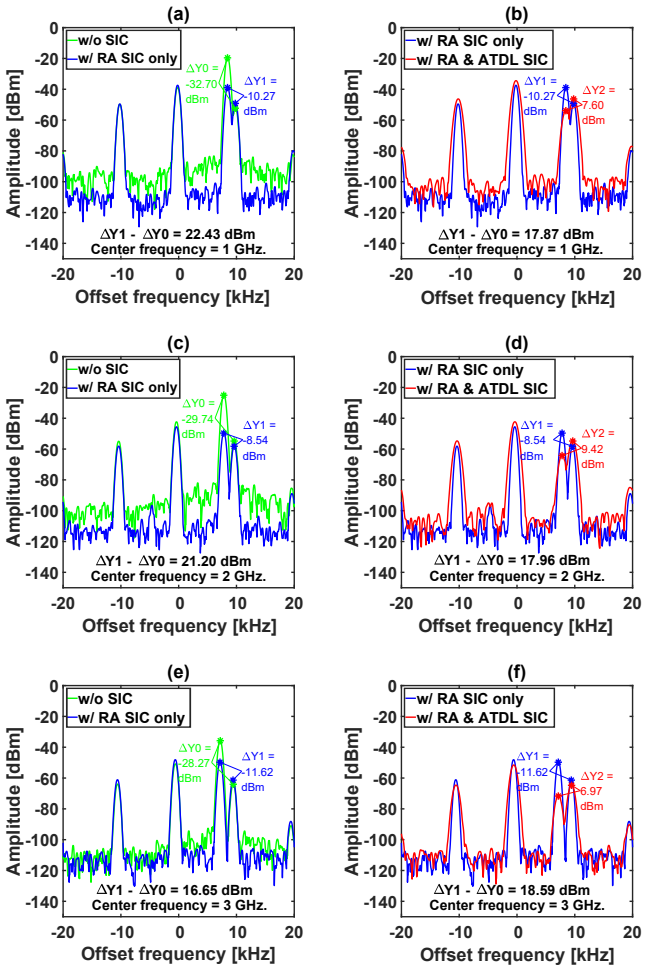


Fig. 19. Measured spectrum of the receive signals using an RF signal analyzer (Keysight 9020A). The first, second, and third rows of plots correspond to AM-modulated receive signals with a carrier frequency equal to 1, 2, and 3 GHz, respectively (TX2 power level of 10 dBm). In each case, a continuous wave (CW) local transmit signal TX1 (at -20 dBm) is applied at an offset of ∼10 kHz from the receiver carrier frequency. The left-hand '*'-marker on each curve shows the peak of this self-interference signal, while the right-hand '*'-marker shows the peak of the high-side AM sideband of the receive signal. The left-hand column shows the improvement in signal-to-interference and noise ratio (SINR) after using only the replica-antenna (RA) SIC, while the right-hand column shows the SINR improvement after applying both SIC stages (the RA and a single-tap ATDL network tuned to the chosen carrier frequency).

(b) show direct measurements of the reference constellations: the remote source TX2 and unwanted local source TX1 use QAM16 and QPSK, respectively, both with symbol rates of 5 MS/s (limited by the spectrum analyzer's limited real-time bandwidth of 25 MHz).

Fig. 23(a) shows the received constellation in FD mode without the SIC when TX1 is set to a moderate power level (−10 dBm). The desired constellation (from the remote source TX2) is effectively randomized by the self-interference, resulting in very high bit error rate (BER). At higher transmit power levels (0 dBm), the received constellation is dominated by the self-interference, as visible in Fig. 23(b).

Next, the experiments were repeated with both the SIC stages (RA and ATDL) enabled; the results are shown in

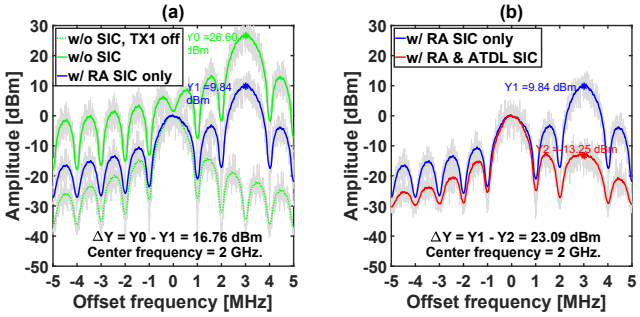


Fig. 20. Measured spectrum of the receive signals using a Keysight MXA signal analyzer (9020A). An 8192-point DFT was performed on the digitally-demodulated QAM16 data to generate this group of figures. In each figure, the carrier frequency of the receive signal is 2 GHz, while that of the transmit signal is offset from it by ∼3 MHz. TX1 and TX2 power levels were set to −5 dBm and 10 dBm, respectively. The modulation type and symbol rate for TX1 and TX2 are 1MS/s QPSK and 1MS/s QAM16, respectively. '*'-markers on every curve show the peak of self-interference caused by the transmit signals in different configurations indicated by the legends. The smooth curves were generated using an average over several scans, while the light gray traces behind them show the original data.

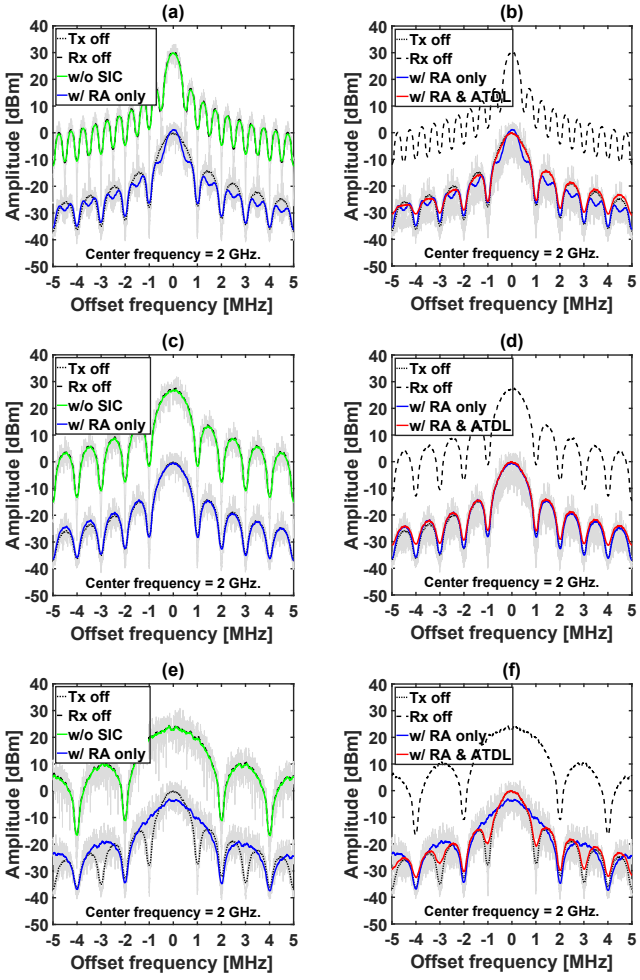


Fig. 21. Received signal spectra (after demodulation) for FD operation with identical transmit (TX1) and receive (TX2) carrier frequencies (both equal to 2 GHz). TX1 used QPSK modulation while TX2 used QAM16 modulation; the symbol rate for the remote transmitter (TX2) was fixed at 1 MS/s, while that for the local transmitter was varied between: (a)-(b) 0.5 MS/s, (c)-(d) 1 MS/s, and (e)-(f) 2 MS/s. TX1 and TX2 power levels were set to −5 dBm and 10 dBm, respectively.

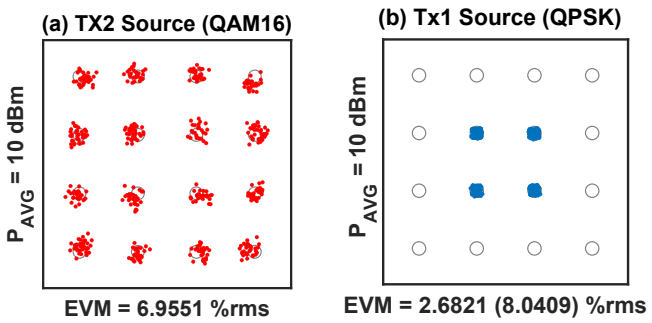


Fig. 22. Measured constellation diagrams (at 2 GHz) by using a signal analyzer (Keysight 9020A) : (a) Direct measurement of the remote source TX2 (10 dBm, QAM16, 5 MS/s). (b) Direct measurement of the unwanted local source TX1 (10 dBm, QPSK, 5 MS/s). The EVM numbers correspond to QAM16 (QPSK) demodulation, respectively.

Figs. 24(a)-(b). The desired signal constellation (from TX2) is clearly visible in both cases, and only a modest increase in error vector magnitude (EVM) is observed even at the higher transmit power level (0 dBm). This result demonstrates the potential of the proposed SIC approach for practical FD antenna arrays.

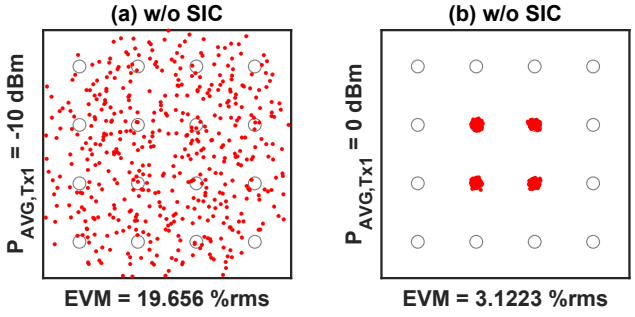


Fig. 23. Measured constellation diagrams in FD mode (at 2 GHz) using a signal analyzer (Keysight 9020A) at the receive port of the dual antenna system without proposed SIC in various situations: (a)-(b) FD measurement of the remote source TX2 (10 dBm, QAM16, 5 MS/s) while TX1 is broadcasting at (a) moderate (−10 dBm) and (b) stronger (0 dBm) signal strengths.

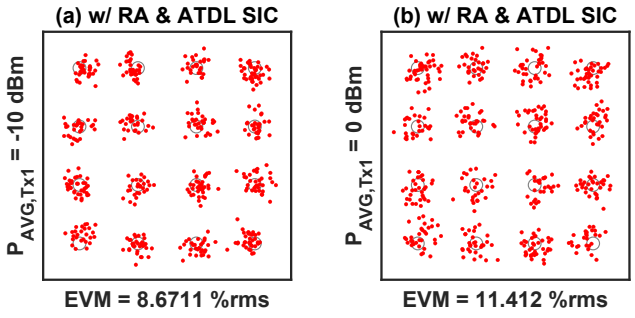


Fig. 24. Measured constellation diagrams in FD mode (at 2 GHz) using a signal analyzer (Keysight 9020A) at the receive port of the dual antenna system using the proposed SIC in various situations: (a)-(b) Remote source TX2 (10 dBm, QAM16, 5 MS/s) measured using both the RA and ATDL SIC while TX1 is broadcasting at (a) moderate (−10 dBm) and (b) stronger (0 dBm) signal strengths.

### *E. Performance Comparison*

Table II compares the performance of the proposed two-stage SIC network with others in the literature. Our design has several advantages, including low hardware complexity, low insertion loss (IL), and wide bandwidth.

TABLE II
FULL-DUPLEX PERFORMANCE COMPARISON WITH PREVIOUS WORK[1].

| Device | Bandwidth (GHz) | Tx-Rx isolation (dB) | Ant-Rx IL (dB) | Technology |
|---|---|---|---|---|
| Proposed | | | | |
| Individual bands | 0.91-1.57 | 63.5-70.6 | 3.6 | RA, ATDL |
| | 1.75-2.39 | 70.4-73.5 | 4.0 | RA, ATDL |
| | 2.90-3.43 | 82.6-90.0 | 4.4 | RA, ATDL |
| Overall | 0.91-3.43 | 63.5-90.0 | 3.6-4.4 | RA, ATDL |
| [28] | 0.45-1 | 40-50 | 1.7-3 | NPF |
| [30] | 0.74-0.77 | 15-50 | 1.7 | NPF |
| [31] | 1-2 | 20-35 | 5-8 | SSDL |
| [6] | 1.15-1.2 | 22-25 | 3-6 | SSDL |
| [29] | 22.7-27.3 | 18-20 | 3.2-4 | STCM |
| [23] | 2.0-2.15 | 55-75 | 3.9 | EBD |

[1] RA: replica antenna; ATDL: analog tapped delay line; NPF: N-path filtering; SSDL: sequentially switched delay line; STCM: spatiotemporal conductivity modulation; EBD: electrically balanced duplexing; IL: insertion loss.

## VI. CONCLUSION

The paper has described a low-complexity two-stage self-interference cancellation (SIC) scheme for full-duplex antenna arrays. The first-stage SIC uses replica antennas for cancellation; the latter acts like an analog computing block that models the mutual coupling between the transmit and receive chains in the presence of the main antennas. Such modeling would be challenging to achieve using a finite-order ATDL finite impulse response filter (FIR) or other lumped circuit because of the need to approximate a high-order transfer function. Thus, using a replica of the main antennas avoids the difficult ATDL design problem by obtaining an exact solution "essentially for free", the trade-offs being increased physical size and insertion losses of ∼3 dB in the transmit and receive paths. In addition, since the proposed replica-antenna canceller is passive, it is linear and distortionless, ultra-wideband (cancellation bandwidth is only limited by that of the couplers and hybrids, resulting in very high DBP), noiseless (apart from loss in the couplers and hybrids), and consumes no power. The second-stage SIC uses a digitally-programmable ATDL network that provides significant additional cancellation at relatively low hardware complexity. Combining the two stages provides excellent Tx/Rx isolation (67-86 dB) and large instantaneous bandwidth (0.53-0.65 GHz) over a multi-octave tuning range (1-3 GHz). These performance metrics, which are significant improvements over the state of the art, demonstrate the promise of the proposed SIC approach for realizing FD MIMO radios.

## REFERENCES

[1] K. Srinivasan, S. Hong, M. Jain, J. I. Choi, J. Mehlman, S. Katti, and P. Levis, "Beyond Full Duplex Wireless," in *Asilomar Conference on Signals, Systems and Computers*, November 2012.

[2] J. I. Choi, M. Jain, K. Srinivasan, P. Levis, and S. Katti, "Achieving Single Channel, Full Duplex Wireless Communication," in *Proceedings of the 16th Annual International Conference on Mobile Computing and Networking (Mobicom 2010)*, September 2010.

[3] M. Biedka, Q. Wu, X. Zou, S. Qin, and Y. E. Wang, "Integrated time-varying electromagnetic devices for ultra-wide band nonreciprocity," in *2018 IEEE Radio and Wireless Symposium (RWS)*, Jan 2018, pp. 80–83.

[4] A. Kord, D. L. Sounas, and A. Alù, "Differential magnetless circulator using modulated bandstop filters," in *2017 IEEE MTT-S International Microwave Symposium (IMS)*, June 2017, pp. 384–387.

[5] A. Kord, M. Tymchenko, D. L. Sounas, H. Krishnaswamy, and A. Alù, "CMOS integrated magnetless circulators based on spatiotemporal modulation angular-momentum biasing," *IEEE Transactions on Microwave Theory and Techniques*, vol. 67, no. 7, pp. 2649–2662, July 2019.

[6] C. F. Campbell, "Demonstration of a sequentially switched delay line (SSDL) circulator with SAW filter delay elements," in *2019 IEEE MTT-S International Microwave Symposium (IMS)*, June 2019, pp. 520–523.

[7] A. Nagulu, T. Chen, G. Zussman, and H. Krishnaswamy, "A single antenna full-duplex radio using a non-magnetic, CMOS circulator with in-built isolation tuning," in *2019 IEEE International Conference on Communications Workshops (ICC Workshops)*, May 2019, pp. 1–6.

[8] N. Reiskarimian, J. Zhou, and H. Krishnaswamy, "A CMOS passive LPTV nonmagnetic circulator and its application in a full-duplex receiver," *IEEE Journal of Solid-State Circuits*, vol. 52, no. 5, pp. 1358–1372, May 2017.

[9] M. Biedka, P. Rodgers, N. Gutierrez, T. LaRocca, and Y. E. Wang, "100MHz to 1GHz on-chip circulator with integrated driver amplifiers," in *2019 IEEE MTT-S International Microwave Symposium (IMS)*, June 2019, pp. 1488–1491.

[10] U. De Silva, H. Malavipathirana, S. Pulipati, S. Bhardwaj, S. Mandal, and A. Madanayake, "Implementation and testing of a switching circulator for twin-pair star radio architectures," in *2020 Moratuwa Engineering Research Conference (MERCon)*, 2020, pp. 331–336.

[11] H. Nawaz and I. Tekin, "Three dual polarized 2.4GHz microstrip patch antennas for active antenna and in-band full duplex applications," in *2016 16th Mediterranean Microwave Symposium (MMS)*, 2016, pp. 1–4.

[12] T. Dinc, A. Chakrabarti, and H. Krishnaswamy, "A 60 GHz same-channel full-duplex CMOS transceiver and link based on reconfigurable polarization-based antenna cancellation," in *2015 IEEE Radio Frequency Integrated Circuits Symposium (RFIC)*, 2015, pp. 31–34.

[13] H. Nawaz and I. Tekin, "Dual-polarized, differential fed microstrip patch antennas with very high interport isolation for full-duplex communication," *IEEE Transactions on Antennas and Propagation*, vol. 65, no. 12, pp. 7355–7360, 2017.

[14] M. J. Cryan, P. S. Hall, S. H. Tsang, and Jizhang Sha, "Integrated active antenna with full duplex operation," *IEEE Transactions on Microwave Theory and Techniques*, vol. 45, no. 10, pp. 1742–1748, 1997.

[15] E. A. Etellisi, M. A. Elmansouri, and D. Filipovic, "Broadband full-duplex monostatic circular-antenna arrays: Circular arrays reaching simultaneous transmit and receive operation," *IEEE Antennas and Propagation Magazine*, vol. 60, no. 5, pp. 62–77, 2018.

[16] U. De Silva, S. Pulipati, S. B. Venkatakrishnan, S. Bhardwaj, and A. Madanayake, "A passive STAR microwave circuit for 1-3 GHz self-interference cancellation," in *2020 IEEE 63rd International Midwest Symposium on Circuits and Systems (MWSCAS)*. IEEE, 2020, pp. 105–108.

[17] L. T. Bruton, *RC active circuits : Theory and design*. Prentice-Hall, 1980.

[18] S. De Silva, M. Okoniewski, and L. Belostotski, "Antenna-array network model," *IEEE Transactions on Antennas and Propagation*, pp. 1–1, 2020.

[19] S. B. Venkatakrishnan, E. A. Alwan, and J. L. Volakis, "Wideband RF self-interference cancellation circuit for phased array simultaneous transmit and receive systems," *IEEE Access*, vol. 6, pp. 3425–3432, 2018.

[20] M. Jain, J. I. Choi, T. Kim, D. Bharadia, S. Seth, K. Srinivasan, P. Levis, S. Katti, and P. Sinha, "Practical, Real-time, Full-Duplex Wireless," in *Proceedings of the 17th Annual International Conference on Mobile Computing and Networking (Mobicom 2011)*, September 2011.

[21] KUMU Networks. [Online]. Available: https://kumunetworks.com/

[22] L. Laughlin, M. A. Beach, K. A. Morris, and J. L. Haine, "Electrical balance duplexing for small form factor realization of in-band full duplex," *IEEE Communications Magazine*, vol. 53, no. 5, pp. 102–110, 2015.

[23] B. van Liempd, B. Hershberg, K. Raczkowski, S. Ariumi, U. Karthaus, K. Bink, and J. Craninckx, "2.2 a +70dBm IIP3 single-ended electrical-balance duplexer in 0.18um SOI CMOS," in *2015 IEEE International Solid-State Circuits Conference - (ISSCC) Digest of Technical Papers*, 2015, pp. 1–3.

[24] E. Manuzzato, J. Tamminen, M. Turunen, D. Korpi, F. Granelli, and M. Valkama, "Digitally-controlled electrical balance duplexer for transmitter-receiver isolation in full-duplex radio," in *European Wireless 2016; 22th European Wireless Conference*, 2016, pp. 1–8.

[25] N. Ginzberg, D. Regev, G. Tsodik, S. Shilo, D. Ezri, and E. Cohen, "A full-duplex quadrature balanced rf front end with digital pre-pa self-interference cancellation," *IEEE Transactions on Microwave Theory and Techniques*, vol. 67, no. 12, pp. 5257–5267, Dec 2019.

[26] K. E. Kolodziej, J. G. McMichael, and B. T. Perry, "Multitap RF canceller for in-band full-duplex wireless communications," *IEEE Transactions on Wireless Communications*, vol. 15, no. 6, pp. 4321–4334, 2016.

[27] D. Regev, N. Ginzberg, and E. Cohen, "Analysis of transmit and receive implementation losses in full duplex wireless transceivers," in *2020 IEEE Texas Symposium on Wireless and Microwave Circuits and Systems (WMCS)*, 2020, pp. 1–5.

[28] N. Reiskarimian and H. Krishnaswamy, "Magnetic-free non-reciprocity based on staggered commutation," *Nature Communications*, vol. 7, no. 1, p. 11217, Apr 2016. [Online]. Available: https://doi.org/10.1038/ncomms11217

[29] T. Dinc, M. Tymchenko, A. Nagulu, D. Sounas, A. Alu, and H. Krishnaswamy, "Synchronized conductivity modulation to realize broadband lossless magnetic-free non-reciprocity," *Nature Communications*, vol. 8, no. 1, p. 795, Oct 2017. [Online]. Available: https://doi.org/10.1038/s41467-017-00798-9

[30] N. Reiskarimian and H. Krishnaswamy, "Fully-integrated non-magnetic non-reciprocal components based on linear periodically-time-varying circuits," in *2017 IEEE 17th Topical Meeting on Silicon Monolithic Integrated Circuits in RF Systems (SiRF)*, 2017, pp. 111–114.

[31] A. M. Darwish, M. Biedka, K. Kingkeo, J. Penn, E. Viveiros, H. A. Hung, and Y. E. Wang, "Multi-octave GaN MMIC circulator for simultaneous transmit receive applications," in *2018 IEEE/MTT-S International Microwave Symposium - IMS*, 2018, pp. 417–419.